2011-07

fac-/mer-[Ru'Cl IND. 3'(NO)(P-N)] (P-N = [o-(N,N-dimethylamino)phenyl]diphenylphosphine): synthesis, characterization and DFT calculations

Inorganica Chimica Acta, Amsterdam : Elsevier, v. 373, n. 1, p. 8-18, July 2011
http://www.producao.usp.br/handle/BDPI/49618

Inorganica Chimica Acta 373 (2011) 8–18

Contents lists available at ScienceDirect

Inorganica Chimica Acta

journal homepage: www.elsevier.com/locate/ica

fac-/*mer*-[$RuCl_3$(NO)(P–N)] (P–N = [*o*-(*N*,*N*-dimethylamino)phenyl]diphenylphosphine): Synthesis, characterization and DFT calculations

Juliana P. da Silva [a], Fabio R. Caetano [a], Deividi A. Cavarzan [a], Francisco D. Fagundes [a], Lincoln L. Romualdo [b], Javier Ellena [c], Maria Jaworska [d], Piotr Lodowski [d], Andersson Barison [a], Márcio P. de Araujo [a,*]

[a] Departamento de Química, Universidade Federal do Paraná, Centro Politécnico, CP 19081, CEP 81531-980, Curitiba (PR), Brazil
[b] Departamento de Química, Universidade Federal de Goiás, Campus Catalão, CEP 75704-020, Catalão (GO), Brazil
[c] Instituto de Física de São Carlos, Universidade de São Paulo, CEP 13560-970, São Carlos (SP), Brazil
[d] Department of Theoretical Chemistry, Institute of Chemistry, University of Silesia, 9th Szkolna Street, 40-006 Katowice, Poland

ARTICLE INFO

Article history:
Received 30 May 2010
Received in revised form 8 March 2011
Accepted 12 March 2011
Available online 21 March 2011

Keywords:
Nitrosyl
Ruthenium
^{15}N-enriched NO
Isomerization
P–N ligand
DFT

ABSTRACT

Complex *fac*-[$RuCl_3$(NO)(P–N)] (**1**) was synthesized from the reaction of [$RuCl_3(H_2O)_2$(NO)] and the P–N ligand, *o*-[(*N*,*N*-dimethylamino)phenyl]diphenylphosphine) in refluxing methanol solution, while complex *mer*,*trans*-[$RuCl_3$(NO)(P–N)] (**2**) was obtained by photochemical isomerization of (**1**) in dichloromethane solution. The third possible isomer *mer*,*cis*-[$RuCl_3$(NO)(P–N)] (**3**) was never observed in direct synthesis as well as in photo- or thermal-isomerization reactions. When refluxing a methanol solution of complex (**2**) a thermally induced isomerization occurs and complex (**1**) is regenerated.

The complexes were characterized by NMR ($^{31}P\{^1H\}$, $^{15}N\{^1H\}$ and ^1H), cyclic voltammetry, FTIR, UV–Vis, elemental analysis and X-ray diffraction structure determination. The $^{31}P\{^1H\}$ NMR revealed the presence of singlet at 35.6 for (**1**) and 28.3 ppm for (**2**). The ^1H NMR spectrum for (**1**) presented two singlets for the methyl hydrogens at 3.81 and 3.13 ppm, while for (**2**) was observed only one singlet at 3.29 ppm. FTIR Ru–NO stretching in KBr pellets or CH_2Cl_2 solution presented 1866 and 1872 cm^{-1} for (**1**) and 1841 and 1860 cm^{-1} for (**2**). Electrochemical analysis revealed a irreversible reduction attributed to Ru^{II}–$NO^+ \rightarrow Ru^{II}$–NO^0 at −0.81 V and −0.62 V, for (**1**) and (**2**), respectively; the process $Ru^{II} \rightarrow Ru^{III}$, as expected, is only observed around 2.0 V, for both complexes.

Studies were conducted using ^{15}NO and both complexes were isolated with ^{15}N-enriched NO. Upon irradiation, the complex *fac*-[$RuCl_3$(NO)(P–N)] (**1**) does not exchange ^{14}NO by ^{15}NO, while complex *mer*,*trans*-[$RuCl_3$(NO)(P–N)] (**2**) does. Complex *mer*,*trans*-[$RuCl_3(^{15}NO)$(P–N)] (**2′**) was obtained by direct reaction of *mer*,*trans*-[$RuCl_3$(NO)(P–N)] (**2**) with ^{15}NO and the complex *fac*-[$RuCl_3(^{15}NO)$(P–N)] (**1′**) was obtained by thermal-isomerization of *mer*,*trans*-[$RuCl_3(^{15}NO)$(P–N)] (**2′**).

DFT calculation on isomer energies, electronic spectra and electronic configuration were done. For complex (**1**) the HOMO orbital is essentially Ru (46.6%) and Cl (42.5%), for (**2**) Ru (57.4%) and Cl (39.0%) while LUMO orbital for (**1**) is based on NO (52.9%) and is less extent on Ru (38.4%), for (**2**) NO (58.2%) and Ru (31.5%).

1. Introduction

Two events have made nitric oxide (NO) one of the most studied small molecules. In 1992, NO was considered the molecule of the year by Science and the 1998s Nobel Prize in physiology or medicine awarded to Robert Furchgott, Ferid Murad and Louis Ignarro for the discovery of NO as a signaling molecule in biological systems. After theses events, an impressive number of works have been published dealing with properties and applications of NO containing transition metal complexes [1–17]. Therefore ruthenium is of crucial importance in the NO chemistry and probably is one of the most studied transition metal with NO in coordination compounds [1–28]. The chemistry of this successful association has been explored by chemists focusing on different aspects. The most explored aspect is the use of such complexes as NO controlled releasing or scavenger compounds [1,2]. Many other insights have been explored, ranging from electronic and molecular structure [3–6,29–33] to catalysis [7–9]. Recently, application of ruthenium–nitrosyl complexes as anticancer agent has emerged [10–13].

In general, ruthenium/nitrosyl complexes are associated with co-ligands such as pyridines [3], salen [2,14], amines [15–18], porphyrins [15,34–39] and diphosphines [12,19–26]. The chemistry of ruthenium/nitrosyl complexes with chelated P–N ligands is rare, and only two works can be found in the literature so far [27,28].

* Corresponding author. Fax: +55 4133613186.
E-mail address: mparaujo@ufpr.br (M.P. de Araujo).

0020-1693/$ - see front matter © 2011 Elsevier B.V. All rights reserved.
doi:10.1016/j.ica.2011.03.042

In this work, we present the synthesis, characterization of *fac/mer*-[$RuCl_3(NO)(P–N)$] (P–N = *o*-[(*N,N*-dimethylamino)phenyl]-diphenylphosphine)). These complexes were characterized by FTIR, NMR ($^{31}P\{^1H\}$, $^{15}N\{^1H\}$, ^1H), cyclic voltammetry, UV–Vis, X-ray diffraction studies and elemental analysis. X-ray structure for (**1**) has been published previously [28], although will be presented to enlighten the discussion. ^{15}N-enriched nitrosyl complexes were also isolated. Density functional theory was also applied in an attempt to understand the electronic structure of these compounds.

2. Experimental methods

2.1. Measurements

The IR spectra were recorded on a FTIR Bomem-Michelson 102 spectrometer in the 4000–400 cm^{-1} region using solid samples pressed in KBr pellets or dichloromethane solution in a CaF_2 crystal with path length of 1 mm. NMR spectra ($^{31}P\{^1H\}$, $^{15}N\{^1H\}$ and ^1H) were acquired at room temperature on a Bruker AVANCE 400 NMR spectrometer, operating at 9.4 T, equipped with a 5 mm multinuclear direct detection probe. The $^{31}P\{^1H\}$ NMR spectra were obtained in CH_2Cl_2 (D_2O capillary was inserted in the solution), while ^1H and $^{15}N\{^1H\}$ NMR spectra were obtained in $CDCl_3$. The ^{31}P, ^{15}N and ^1H NMR chemical shifts are given in parts per million related to H_3PO_4 (85%, capillary), CH_3NO_2 (neat, capillary) and TMS (tetramethylsilane, internal), respectively. The coupling constants are given in Hertz, and the splitting of hydrogen, phosphorus and nitrogen signals are defined as s, singlet; d, doublet; m, multiplet. EPR spectra were measured at 77 K on a Bruker EMX-micro EPR spectrometer, operating at X band, equipped with a rectangular TE_{102} resonator cavity. Cyclic voltammetry (CV) experiments were carried out at room temperature in CH_2Cl_2 or CH_3CN containing 0.1 M $[Bu_4N]ClO_4$ (TBAP) (Fluka Purum) (in these conditions, Half-wave potential for ferrocene is 0.423 V) using a PARC 273 (Princeton Applied Research). The working and auxiliary electrodes were stationary Pt foils; the reference electrode was Ag/AgCl in a Luggin capillary probe filled with the electrolyte solution (TBAP in CH_2Cl_2 or CH_3CN). The electronic spectra were obtained from dichloromethane solution of the complexes in quartz cuvettes with path length of 1 cm, with concentrations ranging from 10^{-6} to 10^{-2} on a Hewlett–Packard diode array 8452A spectrophotometer. The elemental analyses were performed on a Fisons CHNS-O, EA 1108 Element analyser.

Table 1
Crystal data and structures refinement.

	fac-[$RuCl_3(NO)(P–N)$] [28]	*mer,trans*-[$RuCl_3(NO)(P–N)$]
Empirical formula	$C_{20}H_{20}N_2OPCl_3Ru$	$C_{20}H_{20}N_2OPCl_3Ru$
Formula weight	542.77	542.77
Temperature (K)	150(2)	293(2)
Wavelength (Å)	0.71073	0.71073
Crystal system	orthorhombic	orthorhombic
Space group	$P2_12_12_1$	$P2_12_12_1$
Unit cell dimensions		
a (Å)	9.3629(1)	8.7986 (1)
b (Å)	14.6378(2)	15.2385(3)
c (Å)	15.3757(3)	16.2248(2)
Volume (Å^3)	2107.27(6)	2175.38(6)
Z	4	4
D_{calc} (mg/m^3)	1.711	1.657
Absorption coefficient (mm^{-1})	1.214	1.176
F(0 0 0)	1088	1088
Crystal size (mm^3)	0.315 × 0.309 × 0.296	0.47 × 0.23 × 0.15
Theta range for data collection (°)	3.43–27.5	3.42–27.48
Index ranges	$-12 \leqslant h \leqslant 11$ $-19 \leqslant k \leqslant 18$ $-19 \leqslant l \leqslant 19$	$-11 \leqslant h \leqslant 11$ $-19 \leqslant k \leqslant 19$ $-21 \leqslant l \leqslant 18$
Reflections collected	15 860	16 965
Independent reflections	4828 [*R*(int) = 0.0258]	4942 [*R*(int) = 0.0230]
Completeness to theta = 27.5°	99.7%	99.4%
Absorption correction	Gaussian	Gaussian
Maximum and minimum transmission	0.754 and 0.655	0.830 and 0.622
Refinement method	Full-matrix least-squares on F^2	Full-matrix least-squares on F^2
Computing[a]	Collect, HKL Denzo and Scalepack Shelxs-97, Shelxl-97	Collect, HKL Denzo and Scalepack Shelxs-97, Shelxl-97
Data/restraints/parameters	4828/0/256	4942/0/256
Goodness-of-fit on F^2	1.104	1.147
Final *R* índices [$I > 2\sigma(I)$]	R_1 = 0.0231, wR_2 = 0.0565	R_1 = 0.0316, wR_2 = 0.0818
R indices (all data)	R_1 = 0.0238, wR_2 = 0.0569	R_1 = 0.0321, wR_2 = 0.0821
Absolute structure parameter	0.04(2)	−0.03(3)
Extinction coefficient	0.0071(6)	0.0143(10)
Largest difference peak and hole	0.589 and −0.659 e Å^{-3}	2.044 and −0.445 e Å^{-3}

[a] Data collection, data processing, structure solution and structure refinement, respectively.

2.2. X-ray diffraction data

Crystal data for complexes (**1**) and (**2**) (Table 1): formula weight = 542.77, orthorhombic, $P2_12_12_1$. For (**1**) a = 9.3629(1) Å, *b* = 14.6378(2) Å, *c* = 15.3757(3) Å, *V* = 2107.27 Å^3, *Z* = 4, D_{calc} = 1.711 g cm^{-3}, *R*(*wR*) = 0.0231(0.0565) for 15 860 reflections [$I > 2\sigma(I)$], and for (**2**) a = 8.7986(1) Å, *b* = 15.2385(3) Å, *c* = 16.2248(2) Å, *V* = 2175.38 Å^3, *Z* = 4, D_{calc} = 1.657 g cm^{-3}, *R*(*wR*) = 0.0316(0.0818) for 16 965 reflections [$I > 2\sigma(I)$]. X-ray diffraction data collection using the Collect program [40] was performed on an Enraf-Nonius Kappa-CCD diffractometer utilizing graphite-monochromated Mo Kα radiation (0.71073 Å). Final unit cell parameters were based on all reflections. Integration and scaling of the reflections were performed with the HKL Denzo–Scalepack system of programs [41]. A Gaussian absorption correction was applied [42]. The structure was solved by direct methods using shelxs-97 [43]. The model was refined by full-matrix least-squares on F2 with shelxl-97 [44]. All hydrogen atoms were stereochemically positioned and refined with the riding model.

2.3. Method of calculation

Calculations were performed with Gaussian 03 program [45]. The DFT and TDDFT methods were used with the B3LYP functional [46–48]. In the calculations the PCM solvent model was used [49], with dichloromethane (DCM) as the solvent. The PCM calculations were performed on the optimized geometries without solvent. The DGauss DZVP [50] basis sets were employed for ruthenium with two additional polarization f functions with the exponents 1.9472 and 0.7489. These basis sets are of the form (18s12p9d2f)/[6s5p3d2f]. For C, N, O, P, Cl and H the standard 6–31G* basis set was employed. The specified basis set has already been successfully applied to the calculations for other ruthenium complexes [51]. Natural orbital bond (NBO) population analysis [52] was used for calculating the atomic charges, bond orders and for characterization of the Ru–NO bonding. The molecular structures were depicted by the program Molden [53]. Molecular orbitals were drawn with the use of program GopenMol [54].

2.4. Materials and methods

Commercially available $RuCl_3{\cdot}3H_2O$ was donated by Johnson Matthey plc and was used as received. $Na^{15}NO_2$ was purchased from Sigma–Aldrich (ISOTEC) and used as received. $[RuCl_3(H_2O)_2(NO)]$ and [*o*-(*N*,*N*-dimethylamino)phenyl]diphenylphosphine (P–N) were prepared according to the literature methods [20,55]. The NO was generated by reaction of dilute nitric acid (ca. 33%) over copper metal. The NO gas was passed in a trap with saturated solution of NaOH and dried by passing it through a column containing anhydrous $CaC1_2$. ^{15}NO was generated by the reaction of $Na^{15}NO_2$ and 0.1 mol L^{-1} HCl solution.

The solvents were dried before use. All manipulations involving solutions of the complexes were performed under argon atmosphere. Yields are based on the metal.

2.5. Synthesis of (**1**) and (**2**)

The designation *fac* and *mer* refers to the relative position of the chloro ligands, and the designation *trans* and *cis* refers to the relative position of nitrosyl and phosphorus atom to each other.

2.5.1. fac-[$RuCl_3$(NO)(P–N)] (**1**)

To a degassed methanol solution of $[RuCl_3(H_2O)_2(NO)]$ (200 mg, 0.731 mmol) P–N was added (246 mg, 0.806 mmol) and the resulting suspension was refluxed for 3 h, period in which an orange solid is formed. After cooling the suspension to room temperature the orange solid was filtered and washed with methanol (3× 2 mL) and dried under vacuum. Suitable single-crystals were obtained from slow evaporation of dichloromethane solution protected from light. Yield (372 mg, 94%). *Anal.* Calc. for $C_{20}H_{20}N_2OPCl_3Ru.1/2H_2O$: exp. (Calc.) C, 42.40; H, 3.48; N, 5.16. Found: C, 42.84; H, 3.95; N, 5.00%. IR, ν_{NO} 1866 cm^{-1} (KBr) and 1872 cm^{-1} (CH_2Cl_2). UV–Vis (CH_2Cl_2), λ/nm ($\varepsilon/M^{-1}\,cm^{-1}$) 274 ($7.5\times10^5$); 319 ($4.5\times10^3$); 396 (458); 481 (102). $^{31}P\{^1H\}$ NMR (162 MHz, CH_2Cl_2, D_2O capillary) 35.6 ppm (s). ^1H NMR (400 MHz, $CDCl_3$): δ/(ppm) 8.00–7.35 (m, 14H, aromatic hydrogens); 3.81 (s, 3H, NC*H*$_3$); 3.13 (s, 3H, NC*H*$_3$).

2.5.2. mer,trans-[$RuCl_3$(NO)(P–N)] (**2**)

Complex (**1**) (100 mg, 0.366 mmol) was dissolved in CH_2Cl_2 under argon and the resulting orange solution was stirred during 3 days in presence of white light. The resulting green solution was concentrated to ~1 mL and addition of diethylether yield a green solid. Suitable single-crystals were obtained from slow evaporation of dichloromethane solution. Yield (98 mg, 98%). *Anal.* Calcd. for $C_{20}H_{20}N_2OPCl_3Ru$ exp. (Calc.) C, 43.00; H, 3.85; N, 5.10. Found: C, 42.84; H, 3.95; N, 5.00%. IR, ν_{NO} 1841 cm^{-1} (KBr) and 1860 cm^{-1} (CH_2Cl_2). UV–Vis (CH_2Cl_2), λ/nm ($\varepsilon/M^{-1}\,cm^{-1}$), 273 ($5.0\times10^5$); 313 ($5.1\times10^3$); 400 (27); 480 (10); 625 (3.2). $^{31}P\{^1H\}$ NMR (162 MHz, CH_2Cl_2, D_2O capillary) 28.3 ppm (s). ^1H NMR (400 MHz, $CDCl_3$): δ/(ppm) 7.80–7.38 (m, 14H, aromatic hydrogens); 3.29 (s, 6H, NC*H*$_3$).

2.6. Photo-isomerization reaction in the presence of ^{15}NO (*fac* → *mer,trans*)

The procedure was the same used for the synthesis of *mer,trans*-[$RuCl_3$(NO)(P–N)] (**2**), except that the reaction was carried out under ^{15}NO atmosphere. The green solid isolated is a mixture of *mer,trans*-[$RuCl_3$(NO)(P–N)] and *mer,trans*-[$RuCl_3(^{15}NO)$(P–N)]. Spectroscopic data for ^{15}N-enriched complex: FTIR, ν_{NO} 1807 cm^{-1} (KBr) $^{31}P\{^1H\}$ NMR ($CDCl_3$) 28.3 ppm (d) ($2J_{P-N}$ = 75.4 Hz). $^{15}N\{^1H\}$ NMR (40.5 MHz, $CDCl_3$, CH_3NO_2 capillary) −15.6 ppm (d) ($2J_{N-P}$ = 75.4 Hz).

2.7. Thermal-isomerization (*mer,trans* → *fac*)

A degassed methanol solution of *mer,trans*-[$RuCl_3$(NO)(P–N)] (**2**) (50.0 mg, 0.183 mmol) was refluxed for 5 h in absence of light. The resulting solution was concentrated and an orange solid was obtained after addition of diethylether.

The same procedure was conducted using the mixture of *mer,trans*-[$RuCl_3$(NO)(P–N)] and *mer,trans*-[$RuCl_3(^{15}NO)$(P–N)] obtained above. Spectroscopic data for ^{15}N-enriched complex: FTIR, ν 1828 cm^{-1} (KBr) $^{31}P\{^1H\}$ NMR (162 MHz, CH_2Cl_2, D_2O capillary) 35.6 ppm (d) ($2J_{P-N}$ = 4.0 Hz). $^{15}N\{^1H\}$ NMR (40.5 MHz, $CDCl_3$, CH_3NO_2 capillary) −39.5 ppm (d) ($2J_{N-P}$ = 4.0 Hz)

3. Results and discussion

3.1. Synthesis and basic characterization

Complex *fac*-[$RuCl_3$(NO)(P–N)] (**1**) was synthesized from the reaction of $[RuCl_3(H_2O)_2(NO)]$ and *o*-[(*N*,*N*-dimethylamino)-phenyl]diphenylphosphine (P–N) ligand in refluxing methanol. During the reaction, the complex precipitates as an orange solid. Complex *mer,trans*-[$RuCl_3$(NO)(P–N)] (**2**) was synthesized from the isomerization reaction of (**1**) in dichloromethane when exposed to white light. (*Note.* Solution of complex (**1**) is stable for several days when kept in absence of light.) The orange solution of (**1**) starts to change to green after a few hours and after 3 days, complex (**2**) is precipitated with diethyl ether as a green solid (see Scheme 1).

The third possible isomer, *mer,cis*-[$RuCl_3$(NO)(P–N)], in which the nitrosyl is in *trans* position to the nitrogen of P–N ligand, was not observed.

The $^{31}P\{^1H\}$ NMR spectra for (**1**) and (**2**) presented one singlet centered at 35.6 and 28.3 ppm, respectively. The shielding observed on ^{31}P NMR of (**2**) compared to (**1**) can be rationalized in terms of Ru–P bond lengths in both complexes (see Table 2). It is known that in general there is an inverse relationship between Ru–P bond length and ^{31}P NMR chemical shift [56].

In the ^1H NMR spectra, the methyl hydrogens are observed as two singlets at 3.81 and 3.13 ppm for (**1**) and one singlet at 3.29 ppm for (**2**). The deshielding observed for the methyl hydrogens when compared to the free ligand (δ = 2.60 ppm) and the

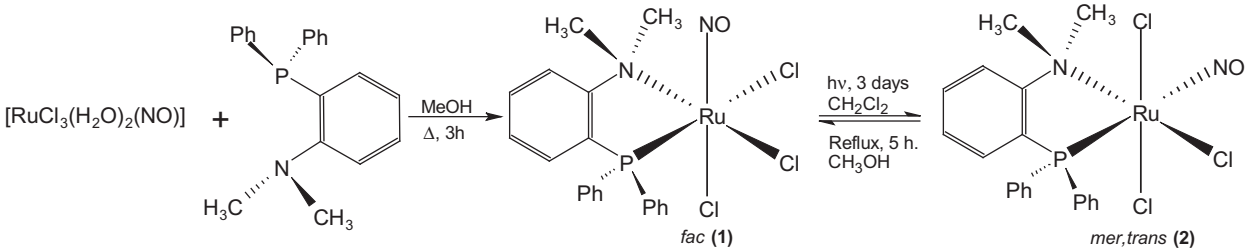

Scheme 1.

Table 2
Selected geometry parameters (calculated and experimental) for complexes **1** and **2**.

	(**1**)		(**2**)	
	Calculated	Exp.	Calculated	Exp.
Bond lengths (Å)				
Ru–N(1)	1.752	1.750(2)	1.766	1.770(3)
Ru–N(2)	2.333	2.2155(18)	2.348	2.222(3)
Ru–P	2.374	2.3241(6)	2.476	2.4038(9)
Ru–Cl(3)	2.364	2.3390(6)	2.374	2.3681(9)
Ru–Cl(1)	2.399	2.3759(6)	2.431	2.3536(8)
Ru–Cl(2)	2.460	2.4153(6)	2.425	2.3710(9)
O–N(1)	1.154	1.135(3)	1.151	1.148(4)
Bond angles (°)				
N(1)–Ru–P	95.50	89.96(6)	177.93	171.45(10)
N(1)–Ru–Cl(3)	176.67	177.64(7)	94.76	93.63(10)
P–Ru–Cl(3)	86.12	87.99(2)	86.70	89.09(3)
N(1)–Ru–Cl(1)	88.08	92.24(7)	93.35	102.79(10)
P–Ru–Cl(1)	92.45	94.56(2)	85.13	85.35(3)
Cl(3)–Ru–Cl(1)	88.95	86.75(2)	91.85	89.07(3)
N(1)–Ru–Cl(2)	87.86	90.84(7)	90.23	84.05(10)
P–Ru–Cl(2)	173.13	174.78(2)	91.25	87.89(3)
Cl(3)–Ru–Cl(2)	90.84	91.31(2)	89.18	89.13(4)
Cl(1)–Ru–Cl(2)	93.66	90.56(2)	176.17	173.03(4)
O–N(1)–Ru	174.37	178.3(2)	178.94	163.7(3)

chemical shifts observed in the $^{31}P\{^{1}H\}$ NMR spectra support a bidentate coordination mode of the P–N ligand.

In the IR spectra, the ν_{NO} band is observed at 1866 cm^{-1} (KBr pellet) and 1872 cm^{-1} (CH_2Cl_2 solution) for complex (**1**), and 1841 cm^{-1} (KBr pellet) and 1860 cm^{-1} (CH_2Cl_2 solution) for complex (**2**). These values are in the range observed for other nitrosyl ruthenium complexes and are characteristics for Ru^{II}–NO^{+} species [10,12,19,20,22,24,57]. For the complexes with ^{15}N-enriched nitrosyl, the ν_{NO} are 1828 and 1807 cm^{-1}, for *fac*-[$RuCl_3$(^{15}NO)(P–N)] (**1′**) and *mer-trans*-[$RuCl_3$(^{15}NO)(P–N)] (**2′**), respectively. These values are shifted to lower energy, 38 and 34 cm^{-1}, for (**1′**) and (**2′**), respectively, when compared to the analogous with ^{14}NO. The values $\nu_{^{14}NO}/\nu_{^{15}NO}$ are 1.021 and 1.019, for (**1′**) and (**2′**), respectively; these values are very close to the theoretical one calculated from the Hooke's Law (1.018) [58].

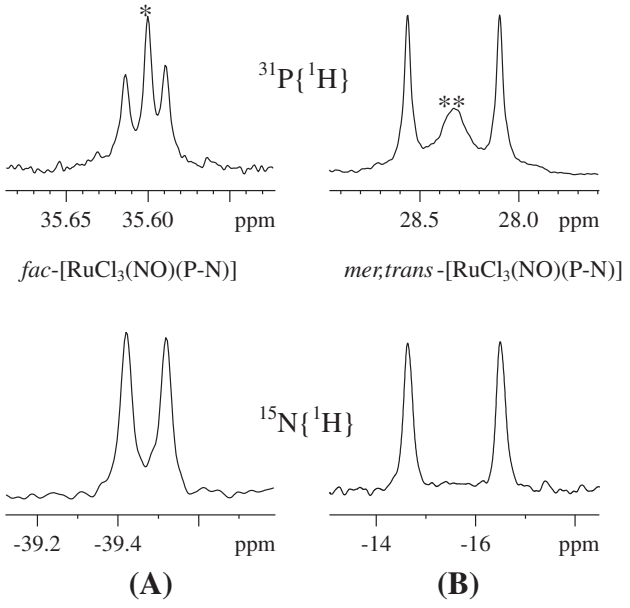

Fig. 1. ^{31}P and ^{15}N NMR ($CDCl_3$) spectra of the mixtures *fac*-[$RuCl_3$(^{14}NO)(P–N)] and *fac*-[$RuCl_3$(^{15}NO)(P–N)] obtained by thermal-isomerization of the mixture of (**2**) and (**2′**) after full conversion (**A**), and *mer,trans*-[$RuCl_3$(^{14}NO)(P–N)] and *mer,trans*-[$RuCl_3$(^{15}NO)(P–N)] obtained by photo-isomerization of (**1**) under 1 atm of ^{15}NO (**B**). ∗Signal for *fac*-[$RuCl_3$(^{14}NO)(P–N)]; ∗∗signal for *mer,trans*-[$RuCl_3$(^{14}NO)(P–N)].

One accepted mechanism for photochemical isomerization of ruthenium nitrosyl complexes involves the dissociation of the NO^0 formed from MLCT ($Ru^{II} \rightarrow NO^{+}$) [59–61]. In order to clarify the mechanism of isomerization (*fac* → *mer,trans*), the isomerization reaction of *fac*-[$RuCl_3$(NO)(P–N] was performed under 1 atm of ^{15}NO. The ^{31}P NMR spectrum was recorded and two signals with the same chemical shift were observed, a singlet and a doublet at 29.3 ppm ($^{2}J_{P-N}$ = 75.4 Hz for the doublet) (see Fig. 1). The singlet corresponds to the complex *mer,trans*-[$RuCl_3$(NO)(P–N)] (**2**) and the doublet corresponds to the complex *mer,trans*-[$RuCl_3$(^{15}NO)(P–N)] (**2′**). The coupling constant is in agreement with phosphorus *trans* to ^{15}N [24,25]. The ^{15}N spectrum NMR revealed a doublet centered at −15.6 ppm ($^{2}J_{N-P}$ = 75.4 Hz) (see Fig. 1). Although this observation indicates a dissociative pathway, the reaction of complex (**2**) with ^{15}NO in the white light also leads to the formation of *mer,trans*-[$RuCl_3$(^{15}NO)(P–N)] (the reaction of (**2**) with ^{15}NO does not occur in the dark). In this way, it is hard to assume that the mechanism is dissociative, once that the reaction can follow another mechanism, for example, via nitrosyl metastable states [62–65] and then, after formation of complex (**2**), the exchange of ^{14}NO by ^{15}NO can occur. It is worth mentioning that complex (**1**) does not exchange ^{14}NO by ^{15}NO in the same conditions, since no complex (**1**) with ^{15}NO was found (the reaction was also analyzed before completion, presenting a mixture of (**1**), (**2**) and (**2′**)). In addition, no paramagnetic species, e.g., Ru^{III} and/or NO^0, were detected by EPR during the isomerization reaction or in the isolated green solid (complex (**2**)). This observation is in accordance with the high yield for the conversion of complex (**1**) into (**2**).

The isomerization proceeds even when carried out in non-degassed dichloromethane or O_2 saturated solution. The isomerization was also conducted in the presence of methanol (CH_2Cl_2:MeOH 2:1) in order to favor the substitution of NO, but no species without NO were observed. Therefore, the dissociation pathway can be discharged, once it would be expected the observation of some denitrosylated species [61].

Irradiating complex (**1**) in dichloromethane with a UV lamp (350 nm/200 W) the isomerization proceeds faster and, as observed previously, without denitrosylation.

On the other hand, complex (**1**) can be obtained refluxing a methanol solution of (**2**) in absence of light (complex (**1**) is thermodynamically more stable than complex (**2**) (see Fig. 4)). The formation of (**1**) was confirmed by $^{31}P\{^{1}H\}$ and ^{1}H NMR. The same procedure was carried out to generate the ^{15}N-enriched complex *fac*-[$RuCl_3$(^{15}NO)(P–N)] (**1′**). Since the precursor was used

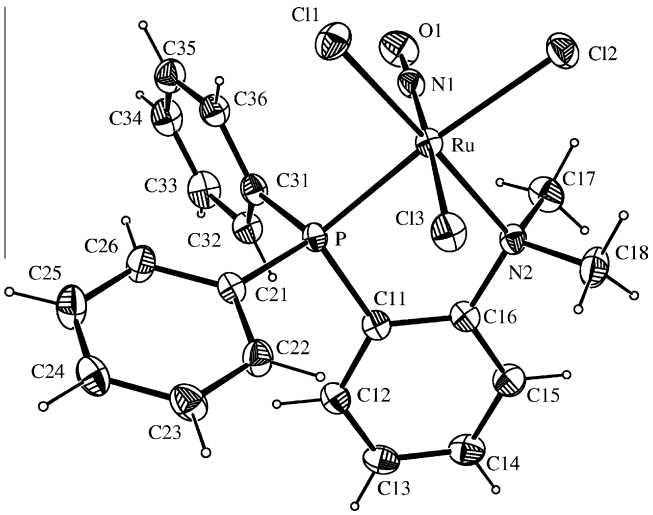

Fig. 2. *ORTEP* view of the complex *fac*-[$RuCl_3$(NO)(P–N)] (**1**), showing the atoms labeling and the 50% probability ellipsoids.

as a mixture of *mer,trans*-[$RuCl_3$(NO)(P–N)] (**2**) and *mer,trans*-[$RuCl_3$(^{15}NO)(P–N)] (**2′**), the *fac* isomer obtained is also a mixture of *fac*-[$RuCl_3$(NO)(P–N)] (**1**) and its ^{15}N-enriched complex (**1′**). The ^{31}P NMR of *fac*-[$RuCl_3$(^{15}NO)(P–N)] presents a singlet and a doublet centered at 35.6 ppm ($^2J_{P-N}$ = 4.0 Hz for the doublet). The ^{15}N spectrum NMR reveals a doublet centered at −39.5 ppm ($^2J_{N-P}$ = 4,0 Hz) (see Fig. 1). Obviously, the singlet belongs to the *fac*-[$RuCl_3$(NO)(P–N)] (**1**) and the doublet to *fac*-[$RuCl_3$(^{15}NO)(P–N)] (**1′**).

In the ^{15}N NMR, the shielding observed for complex (**1′**) when compared to complex (**2′**) is indicative of more linear Ru–N–O for (**1′**) than for (**2′**) which is in agreement with the X-ray structures (see the following section); and the chemical shifts for both complexes are characteristics for Ru^{II}–$^{15}NO^+$ [66].

3.2. X-ray crystallography for complexes (*1*) and (*2*)

Single crystals of complexes (**1**) and (**2**) were obtained by slow evaporation of a dichloromethane solution. Molecular structures of the complexes (**1**) and (**2**) are shown in Figs. 2 and 3, respectively,

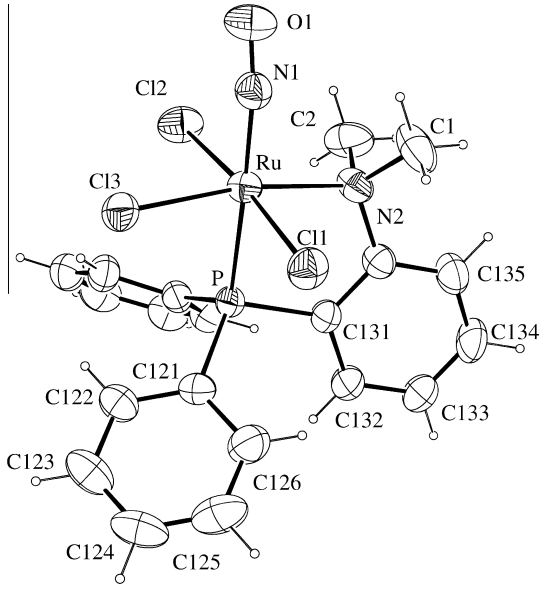

Fig. 3. *ORTEP* view of the complex *mer,trans*-[$RuCl_3$(NO)(P–N)] (**2**), showing the atoms labeling and the 30% probability ellipsoids.

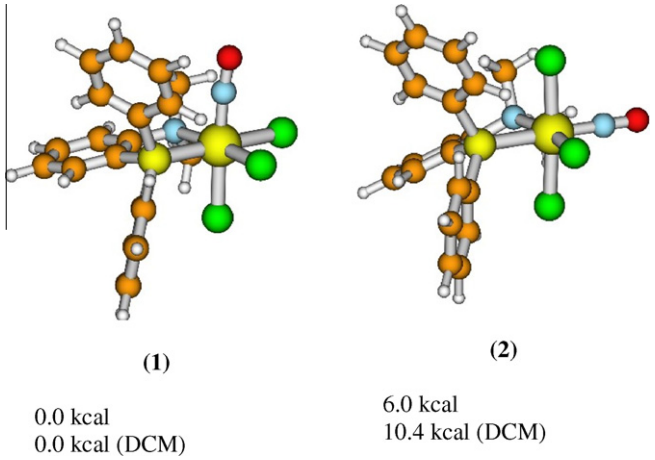

Fig. 4. Optimized geometries and relative energies of the complexes (**1**) and (**2**).

and the relevant bond lengths and angles are summarized in Table 2.

The geometry around ruthenium for both complexes is pseudo-octahedral with the nitrosyl opposite to a chlorine atom in (**1**) and to the phosphorus atom in (**2**). The chlorine atoms adopt a facial configuration in (**1**) and a meridional configuration in (**2**). The Ru–Cl bond lengths are in the range observed in other complexes [10,19,67–72].

Nitrosyl is known to cause a pronounced structural trans-effect (STE) due to its strong π-accepting character, especially when positioned in *trans* position to π-donor or π-acceptor ligands [73]. In complex (**1**), the presence of the nitrosyl in *trans* position to a chlorine atom causes a shortening of the Ru–Cl bond length (Ru–Cl(3) 2.3390(6) Å, *trans* to the NO) when compared to the other two chlorine atoms (Ru–Cl(1) 2.3759(6) Å, *trans* to the N of P–N ligand; Ru–Cl(2) 2.4153(6) Å, *trans* to P). The shortening of Ru–Cl bond is accompanying by shortening of Ru–NO bond, 1.750(2) Å [73].

In complex (**2**), the nitrosyl is in *trans* position to the phosphorus atom and the structural trans-effect (STE) [73] is still observed, but now an elongation of Ru–P bond is observed when compared to (**1**) [Ru–P, 2.3241(6) Å and 2.4038(9) Å in (**1**) and (**2**), respectively]. All Ru–Cl bond lengths are longer in (**2**) (2.3536(8)–2.3710(9) Å) than the Ru–Cl(3) (*trans* to the nitrosyl) observed in (**1**).

Of note is the N–O bond lengths, the presence of π-donor or π-acceptor ligands in *trans* position to nitrosyl also affects the strength of N–O bond. For (**1**), N–O bond length is shorter (1.135(3) Å) than for (**2**) (1.148(4) Å). These distances appear to be the inverse of the expected, since the presence of a π-donor atom should intensify the Ru–NO π-backbonding. Actually, this is not a surprise, and examples can be found in other *mer* complexes [25].

The Ru–N bond length in (**1**) (Ru–N(1) 1.750(2) Å) is shorter than in (**2**) (Ru–N(1) 1.770(3) Å). It is known that for complexes such as *fac/mer*-[$RuCl_3$(NO)(P–P)] [25] the expected behavior for the *mer*- compared to *fac*-isomer, in general, is not observed. In *fac*-isomer, the nitrosyl is opposite to a chlorine atom and due to this arrangement, the Ru–NO π-backbonding interaction should be more favorable when compared to the *mer*-isomer. For the *mer*-isomer, the nitrosyl is opposite to a phosphorus atom (a π-acceptor competitor). The same trend is observed in the *fac/mer,-trans*-[$RuCl_3$(NO)(P–N)] described here. One could expect higher ν_{NO} for complex (**2**) than for (**1**), but this is not observed. In addition, the N–O bond length follows the NO stretching; N–O bond length in (**2**) is longer than in (**1**).

Another aspect worth mentioning is the Ru–N–O bond angles, 178.3(2)° and 163.7(3)° in (**1**) and (**2**), respectively, which is in agreement with the ν_{NO} and ^{15}N{^{1}H}NMR chemical shifts.

3.3. Geometry

The geometry optimization for the complexes (**1**) and (**2**) was carried out without any symmetry constraints. The optimized structures and the relative energies are depicted in Fig. 4. The selected geometry parameters, including the experimental bond lengths and angles, are gathered in Table 2. Complex (**2**), which is a product of the photochemical isomerization, has energy of 6.0 kcal higher than (**1**) in vacuum, in dichloromethane (DCM) this difference becomes 10.4 kcal. The photochemical isomerization leads to the isomer (**2**), the complex with the highest energy. One may note, however, that this is a photochemical reaction, which occurs on the excited state energy surface and, contrary to the thermal rearrangement, it does not need to lead to the lowest energy product. The calculated geometry parameters are in good agreement with the experimental ones. The largest difference between calculated and experimental geometry parameter, over

Table 3
Orbital energies for (**1**) and (**2**). H stands for HOMO, L for LUMO.

Orbital	(**1**)		(**2**)	
Occupied				
117	H-19(σ_{Ph})	−9.68	H-19(d + π^*_{NO})	−9.51
118	H-18(σ_{P-C})	−9.64	H-18(d + π^*_{NO})	−9.50
119	H-17(d + π^*_{NO})	−9.52	H-17(d,Cl)	−9.27
120	H-16(d + π^*_{NO})	−9.30	H-16(σ_{P-C})	−9.23
121	H-15(σ_{P-C})	−9.16	H-15(σ_{P-C})	−9.10
122	H-14(d, Cl)	−9.02	H-14(σ_{P-C})	−9.01
123	H-13(Cl, n_N)	−8.60	H-13(Cl, n_N)	−8.39
124	H-12(Cl, n_N)	−8.37	H-12(n_N, Cl)	−8.31
125	H-11(π_{Ph})	−7.73	H-11(Cl)	−7.70
126	H-10(π_{Ph})	−7.57	H-10(Cl)	−7.62
127	H-9(Cl)	−7.47	H-9(π_{Ph}, Cl)	−7.50
128	H-8(π_{Ph},Cl)	−7.44	H-8(π_{Ph},Cl)	−7.40
129	H-7(Cl, π)	−7.37	H-7(Cl)	−7.28
130	H-6(Cl, π_{Ph})	−7.34	H-6(Cl)	−7.23
131	H-5(π_{Ph}, Cl)	−7.27	H-5(Cl)	−7.12
132	H-4(π_{Ph}, Cl)	−7.20	H-4(π_{Ph})	−7.05
133	H-3(Cl)	−7.14	H-3(π_{Ph})	−6.97
134	H-2(π_{Ph},Cl)	−7.03	H-2(Np, π_{Ph})	−6.88
135	H-1(n_P, Cl)	−7.02	H-1(Cl, π_{Ph})	−6.76
136	H(d, Cl)	−6.69	H(d, Cl)	−6.48
Virtual				
137	L(π^*_{NO}-d)	−3.14	L(π^*_{NO}-d)	−3.10
138	L + 1(π^*_{NO}-d)	−3.09	L + 1(π^*_{NO}-d)	−3.08
139	L + 2(d)	−2.47	L + 2(d)	−2.51
140	L + 3(d)	−1.97	L + 3(d)	−2.08
141	L + 4(σ^*_{P-C})	−1.40	L + 4(σ^*_{P-C})	−1.24
142	L + 5(π^*_{Ph})	−0.95	L + 5(π*)	−0.78
143	L + 6(σ^*_{P-C})	−0.85	L + 6(σ^*_{P-C})	−0.68
144	L + 7(π^*_{Ph})	−0.52	L + 7(σ^*_{P-C})	−0.45
145	L + 8(σ^*_{P-C})	−0.45	L + 8(π^*_{Ph})	−0.27
146	L + 9	−0.31	L + 9(π^*_{Ph})	−0.17

0.1 Å, is found for Ru–N2 bond length. The Ru–NO bond lengths are well reproduced in the calculations; the difference is 0.002 Å for (**1**) and 0.004 Å for (**2**) while the calculated N–O bond lengths are slightly greater than the experimental ones. The differences are approximately 0.02 Å and 0.003 Å for (**1**) and (**2**), respectively. The calculated N–O distance in complex (**2**) is somewhat smaller than in (**1**) and an inverse relationship regarding the experiment is found for these bond lengths. In calculations the Ru–NO and N–O bond lengths are consistent with the concept of a more favored π-backbonding interaction in *fac*-isomer (**1**). Shorter Ru–NO bond and longer N–O bond in the complex (**1**) compared to (**2**) may be associated with a stronger effect of back donation of electrons from d orbital of the ruthenium into π antibonding orbital of NO ligand. The calculated Ru–N–O angle is 174.4° (178.3° experimental) in (**1**) and 178.9° (163.7° experimental) in (**2**). The difference between calculated and experimental bond lengths and bond angle may be a result of a soft energy potential to NO bending, and/or crystal packing forces.

3.4. Molecular orbitals and population analysis

In Table 3, the orbital energies for complexes (**1**) and (**2**) are gathered, and in Fig. 5 selected molecular orbitals are depicted for (**1**) and (**2**). The bonding molecular orbitals of the Ru–NO bond are 119 (HOMO-17), 120 (HOMO-16) for (**1**) and 117, 118 (HOMO-19, HOMO-18) MOs for (**2**). The respective antibonding orbitals are 137, 138 (LUMO, LUMO+1) for both isomers. The bonding orbitals contain admixtures from chlorine and phenyl orbitals. The bonding orbitals are mainly d in character, while the antibonding orbitals are mainly centered on NO. The form of bonding and antibonding orbitals of Ru–NO bond implies that this bond can be described as Ru^{II}–NO^+ type in both isomers.

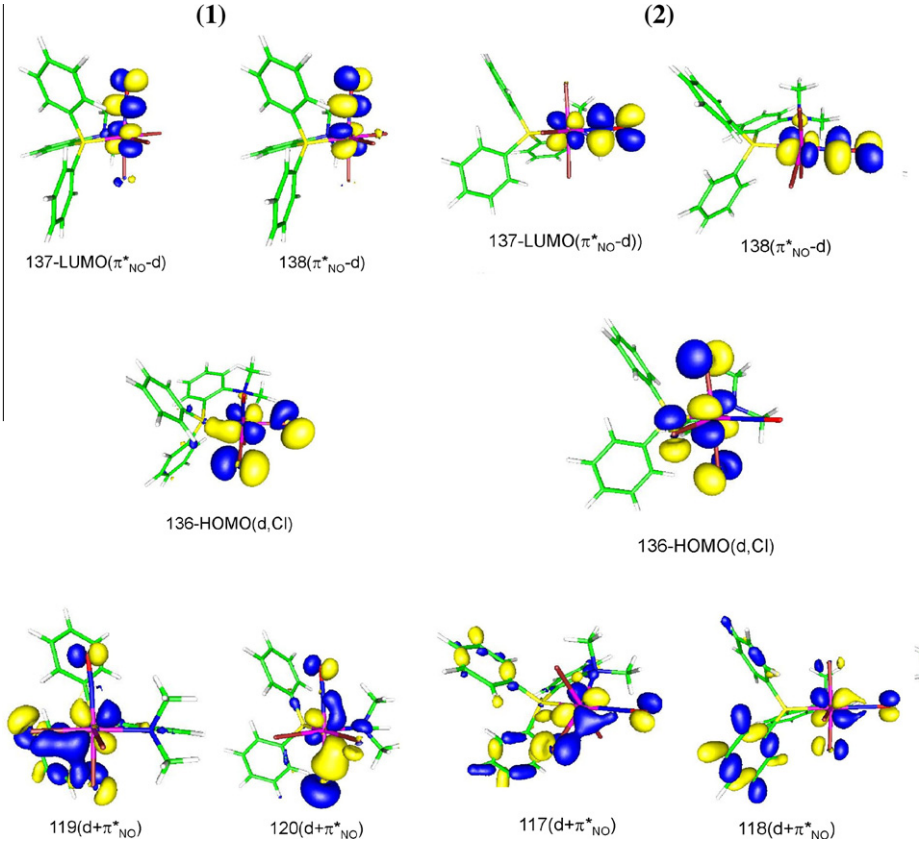

Fig. 5. Selected molecular orbitals of the complexes (**1**) and (**2**).

The orbitals 122(HOMO-14) and 136(HOMO) of (**1**) consist of the ruthenium d_{xy} orbital and π-orbitals of Cl. The low energy d_{xy} orbital is mixed with the occupied π-Cl orbitals, as a result, the HOMO orbital gains significant d character. This effect may be described as a repulsive interaction between d_{xy} and π-Cl occupied orbitals, as a result, the d_{xy} orbital is shifted to higher energy. In (**2**), the respective orbitals are 119 and 136. In complex (**2**), the doubly occupied d orbital interacts with three chlorine orbitals while in (**1**) only with two. As a result, the HOMO orbital of (**2**) is higher in energy than in (**1**) (Table 3). The orbital 135(HOMO-1) of (**1**) is a free electron pair orbital on the phosphorus atom (n_P), with an admixture of a π orbital of the *trans*-Cl atom and a π orbital of a phenyl group. The relevant orbital of (**2**) is 134, where n_P mixes with a π orbital of the *cis*-Cl atom, and an orbital of the *trans*-NO ligand. Orbitals 121 and 141 are examples of σ and σ∗ orbitals of the P–C bonds. There are three bonding (σ) orbitals and three antibonding (σ∗) orbitals in PR_3 ligands [74]. They are formed by p orbitals of the phosphorus atom, two of the bonding (and the corresponding antibonding) orbitals have e(π) symmetry and one has symmetry σ along the Ru–P bond. The antibonding carbon–phosphorus orbitals act as π-accepting orbitals in phosphines. The π∗ orbitals of the nitrosyl ligand also have strong π-accepting properties. In the *cis* position (complex (**1**)), the phosphine and NO orbitals interact with three doubly occupied ruthenium d orbitals, and in the *trans* position (complex (**2**)), only with two. In effect, the ruthenium–phosphorus and ruthenium–nitrosyl bonds in (**1**) are stronger than in (**2**). The Ru–P and Ru–NO bond are longer in (**2**) than in (**1**), which is especially visible for the Ru–P bond. As a consequence, the occupied orbitals involving phosphorus atom are lower in energy in (**1**) than those in (**2**), and the unoccupied d orbitals in (**1**) are higher in energy than in (**2**) (Table 3).

The differences in strengths of Ru–P and Ru–NO bonds for complexes (**1**) and (**2**) can also be seen on the basis of atom–atom overlap-weighted NAO bond order calculations and NBO analysis shown in Tables 4 and 5. The bond orders presented in Table 4 correspond to a sum of off-diagonal NAO density matrix elements between atoms and they can be correlated with the bond strength. In addition, the sum of bond orders on the atoms is also presented. Comparison of the calculated bond orders for Ru–P and Ru–N(1) bonds shows that these bonds are stronger in (**1**) than in (**2**). The stronger binding of ruthenium to P and NO ligand in the complex (**1**) is also evident if one compares the sum value of the bond order for Ru, P and N(1), which are higher just for this isomer. In the case of N–O bond the relation between the indexes for (**1**) and (**2**) is reversed. The value of N–O bond order for complex (**1**) is smaller than for (**2**), and therefore N–O bond in the complex (**1**) should be weakened compared to this bond in the complex (**2**).

Table 4
Atom–atom overlap-weighted NAO bond order for selected bonds of (**1**) and (**2**) complexes in calculations with PCM/DCM solvent model.

	(**1**)	(**2**)
Overlap-weighted NAO bond order		
Ru–P	0.6756	0.6343
Ru–N(1)	1.0033	0.9809
Ru–N(2)	0.3339	0.3315
Ru–Cl(1)	0.5986	0.5911
Ru–Cl(2)	0.5818	0.6015
Ru–Cl(3)	0.6768	0.6171
N(1)–O	1.2879	1.2917
Totals on atom		
Ru	3.7699	3.6645
P	3.2710	3.1813
N(1)	2.3725	2.3152
O	1.2276	1.2279
N(2)	2.6774	2.6758
Cl(1)	0.6579	0.6721
Cl(2)	0.6102	0.6538
Cl(3)	0.7299	0.6730

Table 5
NBO analysis for Ru–N(1) and Ru–P bonds in calculations with PCM/DCM solvent model. (The hybridization is indicated with the percent contribution of the s, p and d orbitals as a superscript).

NBO		Occupancy
*Complex (**1**)*		
	Bonding orbital	
σ(Ru–P)	$0.592(s^{15.51}p^{47.45}d^{36.92})_{Ru} + 0.806(s^{30.07}p^{69.73})_P$ *35.0%* *65.0%*	1.8213
σ(Ru–N(1))	$0.445(s^{13.95}p^{42.84}d^{42.69})_{Ru} + 0.895(s^{65.02}p^{34.97})_{N(1)}$ *19.8%* *80.2%*	1.9345
π_1(Ru–N(1))	$0.802(d^{98.02})_{Ru} + 0.598(p^{99.92})_{N(1)}$ *64.3%* *35.7%*	1.9709
π_2(Ru–N(1))	$0.795(d^{91.47})_{Ru} + 0.606(p^{98.88})_{N(1)}$ *63.2%* *36.8%*	1.9183
	Lone pair	
d_{xy} LP_1(Ru)	$d^{99.76}$	1.9614
*Complex (**2**)*		
	Bonding orbital	
σ(Ru–P)	$0.584(s^{22.97}p^{27.54}d^{49.45})_{Ru} + 0.812(s^{30.50}p^{69.36})_P$ *34.1%* *65.9%*	1.8846
π_1(Ru–N(1))	$0.805(d^{94.55})_{Ru} + 0.592(p^{99.94})_{N(1)}$ *65.0%* *35.0%*	1.9276
π_2(Ru–N(1))	$0.802(d^{98.31})_{Ru} + 0.598(p^{99.94})_{N(1)}$ *64.3%* *35.7%*	1.9613
	Lone pair	
d_{yz} LP_1(Ru)	$d^{99.93}$	1.9762
sp_x LP_1(N(1))	$s^{68.52}p^{31.48}$	1.6235

Stronger binding of ruthenium with nitric oxide in the case of complex (**1**) can also be seen from the NBO analysis. The Ru–N(1) bond in (**1**) is described by an additional σ-symmetry orbital (Table 5). This orbital is formed from spd hybridized orbitals of ruthenium and the sp hybridized orbitals of N(1) and it is strongly localized on the nitrogen atom. Such a σ-donation should increase the strength of Ru–NO bond. The σ-symmetry orbital is not present in the case of complex (**2**) and the relevant electron pair is a lone pair, localized solely on the nitrogen atom. For both complexes the π(Ru–NO) orbitals are localized to a great extent (about 65%) on d orbitals of ruthenium (Table 5). Consequently, the electron density is shifted towards the Ru and the NO ligand gains a positive charge. Formally, Ru–NO bond can be described as Ru^{II}–NO^+ type in both complexes.

This is also confirmed by NPA analysis (Table 6). The total charge of the nitrosyl ligand is positive (0.276 for (**1**) and 0.283 for (**2**) in calculations with PCM/CH_2Cl_2 solvent model) and the charge on the ruthenium is negative in both complexes.

According to the π-backbonding concept, increasing the $d_{Ru} \rightarrow \pi^*_{NO^+}$ donation the bond order in NO ligand decreases and should lead to a low energy ν_{NO}. The ν_{NO} frequencies obtained in calculations with PCM/CH_2Cl_2 solvent model are 1929 cm^{-1} and 1934 cm^{-1} for complexes (**1**) and (**2**), respectively (in gas phase: 1960 cm^{-1} for (**1**) and 1971 cm^{-1} for (**2**)). The Ru–NO π-backbonding interaction, more favorable in *fac*-isomer (**1**) leads to a shift of ν_{NO} band in the direction of lower frequencies compared to the *mer,trans*-isomer (**2**). The calculated values of ν_{NO} are also in good agreement with the presented analysis on strength of Ru–NO and N–O bonds in the investigated complexes, but are not confirmed by the experiment. However, it should be noted that the difference of energy for the ν_{NO} in complexes (**1**) and (**2**) is very small. Depending on the external environment, the geometry of the complexes may undergo changes, which may cause a difference in the relative positions of the ν_{NO} band for the complexes.

Table 6
NPA analysis for the complexes (**1**) and (**2**).

	Charge							
	Ru	N(1)	O(1)	N(2)	P	Cl(1)	Cl(2)	Cl(3)
Vacuum								
(**1**)	−0.145	0.413	−0.168	−0.438	1.328	−0.305	−0.391	−0.286
(**2**)	−0.090	0.424	−0.159	−0.439	1.279	−0.375	−0.366	−0.285
Dichloromethane								
(**1**)	−0.132	0.422	−0.146	−0.428	1.348	−0.365	−0.463	−0.324
(**2**)	−0.079	0.423	−0.140	−0.431	1.287	−0.401	−0.396	−0.345

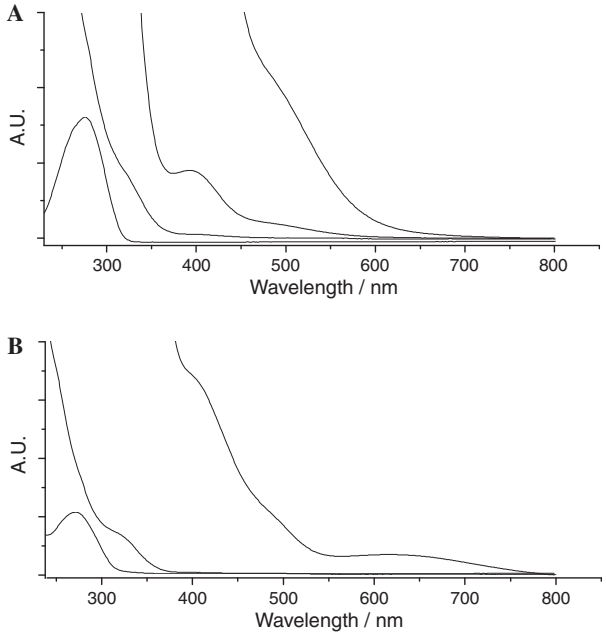

Fig. 6. UV–Vis spectra of *fac*-[$RuCl_3$(NO)(P–N)] (**A**) and *mer,trans*-[$RuCl_3$(NO)(P–N)] (**B**).

Table 7
Electronic spectrum of the complex (**1**) calculated with the TDDFT method in DCM.

ΔE (eV)	λ/nm Calc.	*f*	Excitations	λ/nm (/M^{-1} cm^{-1}) exp.
2.28	543.4	*0.0009*	136(d, Cl) → 137(NO, d)	481 (102)
2.35	526.1	*0.0014*	136(d, Cl) → 138(NO, d)	
2.68	462.2	*0.0049*	136(d, Cl) → 139(d)	
3.02	409.6	*0.0015*	135(P, Cl) → 137(NO, d)	396 (458)
3.10	399.2	*0.0024*	133(Cl) → 138(NO, d) 135(P, Cl) → 138(NO, d)	
3.54	349.4	*0.0071*	129(Cl, π) → 138(NO, d) 131(π) → 138(NO, d)	
3.64	340.0	*0.0303*	134(π, Cl) → 139(d) 135(P, Cl) → 139(d)	319 (sh ∼ 10^3)
3.73	331.8	*0.0202*	129(Cl, π) → 139(d) 133(Cl) → 139(d)	
3.91	316.5	*0.0153*	125(π) → 137(NO, d) 126(π) → 138(NO, d) 129(Cl, π) → 139(d)	
3.96	312.8	*0.0160*	125(π) → 137(NO, d) 130(Cl, π) → 139(d) 135(P, Cl) → 139(d)	
3.97	311.6	*0.0200*	125(π) → 137(NO, d) 130(Cl, π) → 139(d)	
4.07	303.9	*0.0358*	132(π, Cl) → 140(d) 133(Cl) → 140(d)	
4.18	296.3	*0.0852*	124(N, Cl) → 137(NO, d) 134(π, Cl) → 140(d) 135(P, Cl) → 140(d)	
4.22	293.7	*0.0299*	127(Cl) → 139(d) 128(π, Cl) → 139(d) 134(π, Cl) → 140(d)	
4.28	289.4	*0.0303*	124(N, Cl) → 137(NO, d) 130(Cl, π) → 140(d) 135(P, Cl) → 140(d)	
4.50	275.3	*0.1015*	130(Cl, π) → 140(d) 132(π, Cl) → 140(d) 135(P, Cl) → 140(d)	274 (7.5 × 10^5)
4.57	271.0	*0.0389*	125(π) → 139(d)	
4.65	266.1	*0.0221*	136(d, Cl) → 141(σ∗)	

3.5. Electronic spectra

The complex (**1**) has two intense absorptions centered at 274 nm ($\varepsilon = 7.5 \times 10^5$) and 319 nm ($\varepsilon = 4.5 \times 10^3$). In addition, two weak absorptions at 396 nm ($\varepsilon = 458$) and 481 nm ($\varepsilon = 102$) are observed (Fig. 6A). The complex (**2**) has two intense bands at 273 nm ($\varepsilon = 5.0 \times 10^5$) and 313 nm ($\varepsilon = 5.1 \times 10^3$), and three absorptions at 400, 480 and 625 nm with $\varepsilon < 100$ (Fig. 6B). The possible attributions to the observed absorptions can be found in Tables 7 and 8.

The electronic spectra of (**1**) and (**2**) were calculated using the TDDFT method with the PCM solvent model, using DCM as the solvent. The TDDFT excited state wave function is a combination of singly excited determinants, arising from single excitations in the ground state, one-determinant wave function. In Tables 7 and 8, the calculated transition energies, oscillator strengths and the most important excitations (those with the largest coefficients in the excited wave function) are collected for complexes (**1**) and (**2**), respectively. Only those transitions with the largest oscillator strengths are presented, except for the long wave part of the spectrum where the transitions with small oscillator strengths are also shown. In the orbital description used in Tables 7 and 8, N, P, Cl symbols are used for the free electron pairs orbitals, σ denotes a σ_{P-C} orbital and π are phenyl orbitals. d–NO and NO–d are bonding and antibonding orbitals of the nitrosyl metal bond, the former are of predominantly d in character, the later is mostly π^*_{NO} type.

The characteristics intraligand transitions ($\sigma \rightarrow \sigma*$) of coordinated arylphosphines are omitted since the calculated values are below 250 nm.

3.6. Cyclic voltammetry

Cyclic voltammetry studies of (**1**) and (**2**) (Fig. 7A) revealed one monoelectronic and irreversible redox process attributed to Ru^{II}–$NO^+ \rightarrow Ru^{II}$–NO^0, process 1. For complex (**1**), this process occurs at −0.81 V and for (**2**) at −0.62 V. These values are in the range observed for complexes with general formula *fac/mer*-[$RuCl_3$(NO)(P–P)] [25]. For complexes with the unit "$RuCl_3$(NO)" the observation of one irreversible reduction process followed by a chemical reaction is usual [12,19,25]. After the reduction process Ru^{II}–$NO^+ \rightarrow Ru^{II}$–NO^0, a chemical reaction involving production of free chloride, dissociation of NO^0 and formation of Ru^{II} species occurs [25]. These species produced in solution are oxidized in the range 0–1.50 V, as observed in Fig. 7A for the complexes (**1**) and (**2**).

In general, the process Ru^{II}–$NO^+ \rightarrow Ru^{II}$–NO^0 is observed at lower potentials for *fac*-isomer than for the *mer* [25], as found for complexes (**1**) and (**2**). The easier reduction of (**2**) compared to (**1**) is in

Table 8
Electronic spectrum of the complex (**2**) calculated with the TDDFT method in DCM.

ΔE (eV)	λ/nm Calc.	*f*	Excitations	λ/nm (/M^{-1} cm^{-1}) exp.
2.04	607.0	*0.0002*	136(d, Cl) → 138(NO, d) 136(d, Cl) → 139(d)	625 (<100)
2.09	592.4	*0.0001*	136(d, Cl) → 137(NO, d)	
2.18	567.2	*0.0002*	136(d, Cl) → 138(NO, d) 136(d, Cl) → 139(d)	480 (<100)
2.77	447.5	*0.0005*	135(Cl) → 137(NO, d)	
3.14	394.1	*0.0020*	131(Cl) → 138(NO, d) 134(P, π) → 138(NO, d)	400 (<100)
3.19	388.4	*0.0035*	133(π) → 137(NO, d) 135(Cl) → 139(d)	
3.64	340.3	*0.0068*	128(π) → 138(NO, d) 135(Cl) → 140(d)	
3.70	335.0	*0.0084*	131(Cl) → 139(d) 133(π) → 139(d)	
3.72	332.6	*0.0105*	128(π) → 137(NO, d) 128(π) → 138(NO, d)	313 (5.1×10^3)
3.97	312.1	*0.0106*	130(Cl) → 140(d) 134(P, π) → 140(d)	
4.14	299.2	*0.0228*	126(Cl) → 139(d) 128(π) → 139(d)	
4.27	290.0	*0.1223*	133(π) → 140(d) 134(P, π) → 140(d)	
4.30	288.3	*0.0148*	123(Cl, N) → 137(NO, d) 126(Cl) → 139(d)	
4.32	286.8	*0.0308*	126(Cl) → 139(d) 134(P, π) → 140(d)	
4.38	282.5	*0.0214*	129(Cl) → 140(d) 130(Cl) → 140(d) 132(π) → 140(d)	
4.51	274.4	*0.0361*	123(Cl, N) → 138(NO, d) 124(N, Cl) → 137(NO, d)	273 (5.0×10^5)
4.54	273.0	*0.0143*	125(Cl) → 140(d) 127(Cl, π) → 140(d) 128(π) → 140(d)	

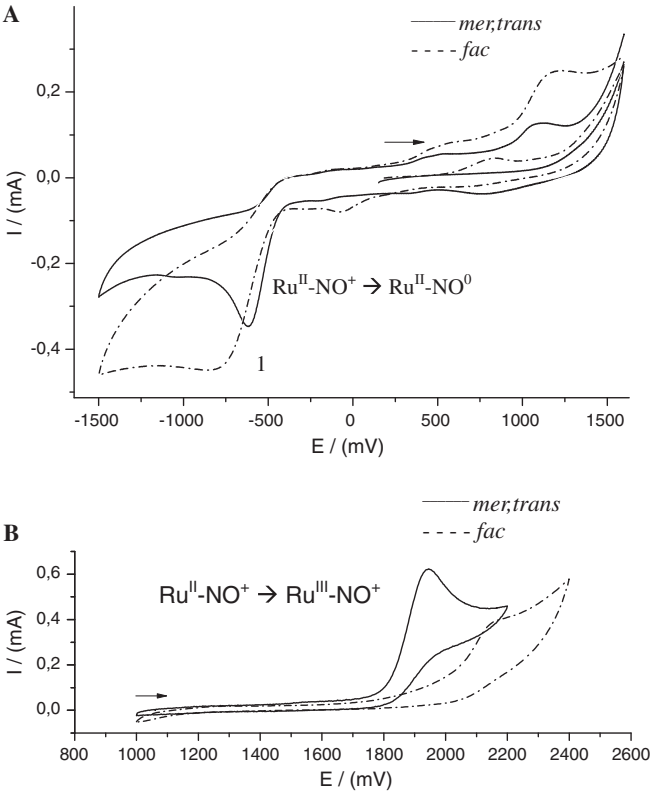

Fig. 7. Cyclic voltammograms for complexes (**1**) and (**2**). Cyclic voltammograms in dichloromethane showing the process centered on NO^+ (**A**). Cyclic voltammograms in acetonitrile showing the process centered on Ru^{2+} (**B**). ([complex] = 1.0×10^{-3} M, in dichloromethane. Pt vs. Ag/AgCl, solution containing PTBA, 0.1 M. Scan rate: 100 mV s^{-1}).

disagreement with ν_{NO}, since a higher NO stretching on infrared spectrum [1872 cm^{-1} for (**1**) and 1860 cm^{-1} for (**2**)] implies in a lower electron density over NO and a lesser cathodic reduction. In addition, the LUMO's energies, −3.14 eV for (**1**) and −3.10 eV in (**2**) are not followed as expected, but as can be noticed, the difference between these two states is small. In both complexes these orbitals are NO predominant, but Ru atomics orbitals have a significant participation. For the complex (**1**), Ru has a participation of 38.4% and NO of 52.9%; for the complex (**2**), Ru has a participation of 31.5% and NO of 58.2%. One explanation for this inversion can be found on the NPA analysis (see Table 6). Analysis of the charges on ruthenium and nitrosyl shows that the charges in (**2**) are ∼0.05 more positive on ruthenium and ∼0.007 on nitrosyl than in (**1**), which is in agreement with the reduction potentials found for both complexes.

The one-electron reduction processes for complex (**1**) and (**2**) can be represented showing the spectator ligand in *trans* position to the NO^+ in both complexes as follow:

$$Cl{-}Ru^{II}{-}NO^+ + e^- \rightarrow Cl{-}Ru^{II}{-}NO^0 \text{ complex} \quad (1)$$

$$P{-}Ru^{II}{-}NO^+ + e^- \rightarrow P{-}Ru^{II}{-}NO^0 \text{ complex} \quad (2)$$

Another aspect that can explain the observed reduction potentials is the arrangement of the ligands in *trans* position to the NO^+. The presence of phosphorus atom in opposite position to the NO^+ in complex (**2**), can lead to a more delocalized system, due to the π-accepting ability of the aromatic substituted phosphines, which can withdraw the additional electron density after the reduction process. On the other hand, the presence of a chlorine atom in *trans* position to the NO^+ in complex (**1**), increases the electron density over NO (see Table 6) leading to a lower reduction process when compared with complex (**2**).

As expected, due to the NO^+ ability to withdraw electron-density from the ruthenium, the process $Ru^{II} \rightarrow Ru^{III}$ for both complexes is only observed at high potential (>1.80 V) (Fig. 7B). For complex (**1**), the metal center is oxidized at 2.19 V and for complex (**2**) this process is observed at 1.95 V. This observation does not follow the expected order considering the NBO charge of ruthenium in both complexes. Although, considering the arrangement of the ligands around the ruthenium; the presence of two π-accepting ligands in opposite position (P from P–N ligand and NO^+) for complex (**2**) can lead to an electron richer ruthenium center when compared to complex (**1**). In addition, HOMO orbital for complex (**2**) is higher in energy than the HOMO for complex (**1**) (see Table 3), which is in accordance with the observed potentials for the process $Ru^{II} \rightarrow Ru^{III}$.

Comparison among complexes such as *fac/mer*-[$RuCl_3$(NO)(P–P)] [25] and the complexes *fac/mer*-[$RuCl_3$(NO)(P–N)] shows that the presence of a nitrogen instead of a P atom does not cause any significant difference on electrochemical behavior and in the reductions potentials. For example, *fac/mer*-[$RuCl_3$(NO)(dppe)] have the Ru^{II}–$NO^+ \rightarrow Ru^{II}$–NO^0 at −0.87 (*fac*) and −0.70 V (*mer*), and $Ru^{II} \rightarrow Ru^{III}$ at 2.03 (*fac*) and 1.88 V (*mer*); as mentioned before, these values are very similar to the observed for the complexes reported in this work.

4. Conclusions

Two isomers of the complex $[RuCl_3(NO)(P–N)]$ were isolated and studied. Both complexes can be described as $[Ru^{II}–NO^+]^6$. X-ray structures of both complexes were presented and the bond lengths and angles are compatibles to other complexes observed in the literature. The reduction processes are centered at LUMO orbitals which are essentially dominated by orbitals of the NO^+ ligand, but ruthenium has an expressive participation in both complexes. Oxidation processes are observed at high potentials due to the presence of a strong π-acceptor ligand, NO^+. These oxidations processes are centered at HOMO orbitals which are dominated by ruthenium orbitals. Isomerization studies, including formation of ^{15}N-enriched complexes for both isomers and the lack of observation of denitrosylated species exclude the mechanism involving dissociation and recombination of NO^0 during the isomerization process (further studies will be conducted to unravel the mechanism of isomerization, including other ruthenium nitrosyl trihalides).

Acknowledgements

The authors are grateful to CNPq, CAPES and FINEP for financial support and Johnson Matthey plc for the loan of $RuCl_3$ (to M.P.A.). The Gaussian 03 calculations were carried out in the Wrocław Centre for Networking and Supercomputing, WCSS, Wrocław, Poland, under calculational Grant No. 51/96.

Appendix A. Supplementary material

Crystallographic data (excluding structure factors) for complexes (**1**) and (**2**) have been deposited with the Cambridge Crystallographic Data Centre as supplementary publication on CCDC 610163 and 776309, respectively. Copies of the data can be obtained, free of charge via www.ccdc.cam.ac.uk/conts/retrieving.html (or from the Cambridge Crystallographic Data Centre, CCDC, 12 Union Road, Cambridge CB2 1EZ, UK; fax: +44 1223 336033; or e-mail: deposit@ccdc.cam.ac.uk).

References

[1] D. Bonaventura, F.D. Oliveira, V. Togniolo, A.C. Tedesco, R.S. da Silva, L.M. Bendhack, Nitric Oxide 10 (2004) 83.
[2] J. Bordini, P.C. Ford, E. Tfouni, Chem. Commun. (2005) 4169.
[3] O. Lyubimova, O.V. Sizova, C. Loschen, G. Frenking, J. Mol. Struct. (THEOCHEM) 865 (2008) 28.
[4] O.V. Sizova, N.V. Ivanova, O.O. Lyubimova, V.V. Sizov, Russ. J. Coord. Chem. 33 (2007) 523.
[5] O.V. Sizova, L.V. Skripnikov, A.Y. Sokolov, N.V. Ivanova, Russ. J. Coord. Chem. 33 (2007) 588.
[6] O.V. Sizova, A.Y. Sokolov, L.V. Skripnikov, V.I. Baranovski, Polyhedron 26 (2007) 4680.
[7] Y. Cheng, J.F. Sun, H.L. Yang, H.J. Xu, Y.Z. Li, X.T. Chen, Z.L. Xue, Organometallics 28 (2009) 819.
[8] H.J. Xu, Y. Cheng, J.F. Sun, B.A. Dougan, Y.Z. Li, X.T. Chen, Z.L. Xue, J. Organomet. Chem. 693 (2008) 3851.
[9] H.J. Xu, X.Y. Lu, Y. Cheng, J.F. Sun, X.T. Chen, Z.L. Xue, Organometallics 28 (2009) 6687.
[10] C.C. Golfeto, G. Von Poelhsitz, H.S. Selistre-de-Araujo, M.P. de Araujo, J. Ellena, E.E. Castellano, L.G.L. Lopes, I.S. Moreira, A.A. Batista, J. Inorg. Biochem. 104 (2010) 489.
[11] B. Serli, E. Zangrando, T. Gianfeffara, L. Yellowlees, E. Alessio, Coord. Chem. Rev. 245 (2003) 73.
[12] G. Von Poelhsitz, A.L. Bogado, M.P. de Araujo, H.S. Selistre-de-Araujo, J. Ellena, E.E. Castellano, A.A. Batista, Polyhedron 26 (2007) 4707.
[13] F.B. do Nascimento, G. Von Poelhsitz, F.R. Pavan, D.N. Sato, C.Q.F. Leite, H.S. Selistre-De-Araujo, J. Ellena, E.E. Castellano, V.M. Deflon, A.A. Batista, J. Inorg. Biochem. 102 (2008) 1783.
[14] Z.N. da Rocha, M.S.P. Marchesi, J.C. Molin, C.N. Lunardi, K.M. Miranda, L.M. Bendhack, P.C. Ford, R.S. da Silva, Dalton Trans. (2008) 4282.
[15] M.J. Rose, P.K. Mascharak, Coord. Chem. Rev. 252 (2008) 2093.
[16] R.Z. de Osti, D.W. Franco, Polyhedron 26 (2007) 4746.
[17] L.G.F. Lopes, E.E. Castellano, A.G. Ferreira, C.U. Davanzo, M.J. Clarke, D.W. Franco, Inorg. Chim. Acta 358 (2005) 2883.
[18] P.G. Zanichelli, H.F.G. Estrela, R.C. Spadari-Bratfisch, D.M. Grassi-Kassisse, D.W. Franco, Nitric Oxide 16 (2007) 189.
[19] G. Von Poelhsitz, M.P. de Araujo, L.A.A. de Oliveira, S.L. Queiroz, J. Ellena, E.E. Castellano, A.G. Ferreira, A.A. Batista, Polyhedron 21 (2002) 2221.
[20] A.A. Batista, C. Pereira, S.L. Queiroz, L.A.A. de Oliveira, R.H.D. Santos, M.T.D. Gambardella, Polyhedron 16 (1997) 927.
[21] A.A. Batista, C. Pereira, K. Wohnrath, S.L. Queiroz, R.H.D. Santos, M.T.D. Gambardella, Polyhedron 18 (1999) 2079.
[22] G. Von Poelhsitz, A.A. Batista, E.E. Castellano, J. Ellena, Inorg. Chem. Commun. 9 (2006) 773.
[23] G. Von Poelhsitz, A.A. Batista, J. Ellena, E.E. Castellano, E.S. Lang, Inorg. Chem. Commun. 8 (2005) 805.
[24] G. Von Poelhsitz, A.L. Bogado, G.D. de Souza, E. Rodrigues, A.A. Batista, M.P. de Araujo, Inorg. Chem. Commun. 10 (2007) 133.
[25] G. Von Poelhsitz, R.C. de Lima, R.M. Carlos, A.G. Ferreira, A.A. Batista, A.S. de Araujo, J. Ellena, E.E. Castellano, Inorg. Chim. Acta 359 (2006) 2896.
[26] R.C.L. Zampieri, G. Von Poelhsitz, A.A. Batista, O.R. Nascimento, J. Ellena, E.E. Castellano, J. Inorg. Biochem. 92 (2002) 82.
[27] A.A. Batista, S.L. Queiroz, P.C. Healy, R.W. Buckley, S.E. Boyd, S.J. Berners-Price, E.E. Castellano, J. Ellena, Can. J. Chem. 79 (2001) 1030.
[28] D.A. Cavarzan, F.R. Caetano, L.L. Romualdo, F.B. Do Nascimento, A.A. Batista, J. Ellena, A. Barison, M.P. de Araujo, Inorg. Chem. Commun. 9 (2006) 1247.
[29] F. Bottomley, Coord. Chem. Rev. 26 (1978) 7.
[30] G.B. Richter-Addo, P. Legzdins, Metal Nitrosyls, Oxford University Press, New York, 1992.
[31] J.A. McCleverty, Chem. Rev. 104 (2004) 403.
[32] G.F. Caramori, G. Frenking, Croat. Chem. Acta 82 (2009) 219.
[33] G.F. Caramori, G. Frenking, Organometallics 26 (2007) 5815.
[34] G.B. Yi, M.A. Khan, G.B. Richter-Addo, Inorg. Chem. 35 (1996) 3453.
[35] K.M. Kadish, V.A. Adamian, E. Van Caemelbecke, Z. Tan, P. Tagliatesta, P. Bianco, T. Boschi, G.B. Yi, M.A. Khan, G.B. Richter-Addo, Inorg. Chem. 35 (1996) 1343.
[36] N. Xu, J. Lee, D.R. Powell, G.B. Richter-Addo, Inorg. Chim. Acta 358 (2005) 2855.
[37] J.Y. Lee, G.B. Richter-Addo, J. Inorg. Biochem. 98 (2004) 1247.
[38] T. Gianferrara, B. Serli, E. Zangrando, E. Iengo, E. Alessio, New J. Chem. 29 (2005) 895.
[39] D.S. Bohle, P.A. Goodson, B.D. Smith, Polyhedron 15 (1996) 3147.
[40] P. Coppens, L. Leiserow, D. Rabinovi, Acta Crystallogr. 18 (1965) 1035.
[41] Enraf-Nonius, COLLECT, Nonius BV, Delft, The Netherlands, 1997–2000.
[42] Z. Otwinowski, W. Minor, HKL Denzo and Scalepack, in: C.W. Carter Jr., R.M. Sweet (Eds.), Methods in Enzymology, vol. 276, Academic Press, New York, 1997, pp. 307–326.
[43] G.M. Sheldrick, Acta Crystallogr. A 64 (2008) 112.
[44] L.J. Farrugia, J. Appl. Crystallogr. 30 (1997) 565.
[45] M.J. Frisch, G.W. Trucks, H.B. Schlegel, G.E. Scuseria, M.A. Robb, J.R. Cheeseman, J.A. Montgomery Jr., T. Vreven, K.N. Kudin, J.C. Burant, J.M. Millam, S.S. Iyengar, J. Tomasi, V. Barone, B. Mennucci, M. Cossi, G. Scalmani, N. Rega, G.A. Petersson, H. Nakatsuji, M. Hada, M. Ehara, K. Toyota, R. Fukuda, J. Hasegawa, M. Ishida, T. Nakajima, Y. Honda, O. Kitao, H. Nakai, M. Klene, X. Li, J.E. Knox, H.P. Hratchian, J.B. Cross, V. Bakken, C. Adamo, J. Jaramillo, R. Gomperts, R.E. Stratmann, O. Yazyev, A.J. Austin, R. Cammi, C. Pomelli, J.W. Ochterski, P.Y. Ayala, K. Morokuma, G.A. Voth, P. Salvador, J.J. Dannenberg, V.G. Zakrzewski, S. Dapprich, A.D. Daniels, M.C. Strain, O. Farkas, D.K. Malick, A.D. Rabuck, K. Raghavachari, J.B. Foresman, J.V. Ortiz, Q. Cui, A.G. Baboul, S. Clifford, J. Cioslowski, B.B. Stefanov, G. Liu, A. Liashenko, P. Piskorz, I. Komaromi, R.L. Martin, D.J. Fox, T. Keith, M.A. Al-Laham, C.Y. Peng, A. Nanayakkara, M. Challacombe, P.M.W. Gill, B. Johnson, W. Chen, M.W. Wong, C. Gonzalez, J.A. Pople, Gaussian 03, Revision C.02, Gaussian, Inc., Wallingford, CT, 2004.
[46] A.D. Becke, J. Chem. Phys. 98 (1993) 5648.
[47] C.T. Lee, W.T. Yang, R.G. Parr, Phys. Rev. B 37 (1988) 785.
[48] M.E. Casida, C. Jamorski, K.C. Casida, D.R. Salahub, J. Chem. Phys. 108 (1998) 4439.
[49] M. Cossi, V. Barone, R. Cammi, J. Tomasi, Chem. Phys. Lett. 255 (1996) 327.
[50] N. Godbout, D.R. Salahub, J. Andzelm, E. Wimmer, Can. J. Chem. 70 (1992) 560.
[51] J.G. Malecki, R. Kruszynski, M. Jaworska, P. Lodowski, Z. Mazurak, J. Organomet. Chem. 693 (2008) 1096.
[52] A.E. Reed, L.A. Curtiss, F. Weinhold, Chem. Rev. 88 (1988) 899.
[53] G. Schaftenaar, J.H. Noordik, J. Comput. Aided Mol. Des. 14 (2000) 123.
[54] D.L. Bergman, L. Laaksonen, A. Laaksonen, J. Mol. Graphics Modell. 15 (1997) 301.
[55] H.P. Fritz, I.R. Gordon, K.E. Schwarzhans, L.M. Venanzi, J. Chem. Soc. (Resumed) (1965) 5210.
[56] S.L. Queiroz, A.A. Batista, G. Oliva, M. Gambardella, R.H.A. Santos, K.S. MacFarlane, S.J. Rettig, B.R. James, Inorg. Chim. Acta 267 (1998) 209.
[57] G. Aullon, S. Alvarez, R. Cao, M. Ortiz, A.M. Diaz-Garcia, Inorg. Chim. Acta 362 (2009) 4651.
[58] D.A. Freedman, D.E. Janzen, J.L. Vreeland, H.M. Tully, K.R. Mann, Inorg. Chem. 41 (2002) 3820.
[59] J.E. Fergusson, R.K. Coll, Inorg. Chim. Acta 207 (1993) 191.
[60] E. Miki, H. Masano, H. Iwasaki, H. Tomizawa, K. Mizumachi, T. Ishimori, M. Tanaka, T. Nagai, N. Nagao, Inorg. Chim. Acta 205 (1993) 129.
[61] F. Harada, T. Onozuka, H. Tomizawa, M. Tanaka, E. Miki, Inorg. Chim. Acta 359 (2006) 665.

[62] Y. Morioka, A. Ishikawa, H. Tomizawa, E. Miki, J. Chem. Soc., Dalton Trans. (2000) 781.
[63] D.V. Fomitchev, K. Culp, P. Coppens, Abstr. Papers Am. Chem. Soc. 216 (1998) 192-INOR.
[64] D.V. Fomitchev, P. Coppens, T.S. Li, K.A. Bagley, L. Chen, G.B. Richter-Addo, Chem. Commun. (1999) 2013.
[65] S.C. Da Silva, D.W. Franco, Spectrochim. Acta A Mol. Biomol. Spectrosc. 55 (1999) 1515.
[66] J. Mason, L.F. Larkworthy, E.A. Moore, Chem. Rev. 102 (2002) 913.
[67] S.L. Queiroz, A.A. Batista, M.P. De Araujo, R.C. Bianchini, G. Oliva, J. Ellena, B.R. James, Can. J. Chem. 81 (2003) 1263.
[68] A.A. Batista, J. Zukerman-Schpector, O.M. Porcu, S.L. Queiroz, M.P. Araujo, G. Oliva, D.H.F. Souza, Polyhedron 13 (1994) 689.
[69] M.P. de Araujo, A.T. de Figueiredo, A.L. Bogado, G. Von Poelhsitz, J. Ellena, E.E. Castellano, C.L. Donnici, J.V. Comasseto, A.A. Batista, Organometallics 24 (2005) 6159.
[70] M.P. de Araujo, O.M. Porcu, A.A. Batista, G. Oliva, D.H.F. Souza, M. Bonfadini, O.R. Nascimento, J. Coord. Chem. 54 (2001) 81.
[71] M.P. de Araujo, E.M.A. Valle, J. Ellena, E.E. Castellano, E.N. dos Santos, A.A. Batista, Polyhedron 23 (2004) 3163.
[72] L.R. Dinelli, A.A. Batista, K. Wohnrath, M.P. de Araujo, S.L. Queiroz, M.R. Bonfadini, G. Oliva, O.R. Nascimento, P.W. Cyr, K.S. MacFarlane, B.R. James, Inorg. Chem. 38 (1999) 5341.
[73] B.J. Coe, S.J. Glenwright, Coord. Chem. Rev. 203 (2000) 5.
[74] A. Vogler, H. Kunkely, Coord. Chem. Rev. 230 (2002) 243.